ADVANCED MATERIALS INTERFACES
www.advmatinterfaces.de

Detection of Neurofilament Light Chain with Label-Free Electrolyte-Gated Organic Field-Effect Transistors

Kateryna Solodka, Marcello Berto, Diana Ferraro, Claudia Menozzi, Marco Borsari, Carlo A. Bortolotti, Fabio Biscarini, and Marcello Pinti**

Neurofilaments are structural scaffolding proteins of the neuronal cytoskeleton. Upon axonal injury, the neurofilament light chain (NF-L) is released into the interstitial fluid and eventually reaches the cerebrospinal fluid and blood. Therefore, NF-L is emerging as a biomarker of neurological disorders, including neurodegenerative dementia, Parkinson's disease, and multiple sclerosis. It is challenging to quantify NF-L in bodily fluids due to its low levels. This work reports the detection of NF-L in aqueous solutions with an organic electronic device. The biosensor is based on the electrolyte-gated organic field-effect transistor (EGOFET) architecture and can quantify NF-L down to sub-pM levels; thanks to modification of the device gate with anti-NF-L antibodies imparted with potentially controlled orientation. The response is fitted to the Guggenheim–Anderson–De Boer adsorption model to describe NF-L adsorption at the gate/electrolyte interface, to consider the formation of a strongly adsorbed protein layer bound to the antibody and the formation of weakly bound NF-L multilayers, an interpretation which is also backed up by morphological characterization via atomic force microscopy. The label-free, selective, and rapid response makes this EGOFET biosensor a promising tool for the diagnosis and monitoring of neuronal damages through the detection of NF-L in physio-pathological ranges.

1. Introduction

In recent years, neurofilament light chain (NF-L), a neuronal structural protein, has emerged as a potential biomarker of axonal damage in numerous neurological disorders, including neurodegenerative dementia, traumatic brain injury, amyotrophic lateral sclerosis, Parkinson's disease, and multiple sclerosis (MS).[1,2] Neurofilaments (NFs) are structural scaffolding proteins of the axonal cytoskeleton, belonging to the IV class of intermediate filaments that, according to their molecular weight, are classified into neurofilament heavy chain (NF-H, ≈200 kDa), neurofilament medium chain (NF-M, ≈145 kDa), and NF-L (≈68 kDa). All NF proteins are formed by a central α-helical rod region, a variable N-terminal domain, and a C-terminal tail highly variable in length.[3,4] NF monomers form parallel heterodimers through the association of the central rod region. Then, two dimers form an antiparallel tetramer, and eight tetramers associate in a cylindrical structure, which is the minimal repetitive unit of the neurofilament. Together with microfilaments (≈6–8 nm) and microtubules (≈24 nm), neurofilaments (≈10 nm) form the neuronal cytoskeleton, providing structural support to the cell.[4,5] The normal structure and assembled network of NFs is essential for neuronal function, as it has been shown that mutations in NF-L leading to protein aggregation or to a complete absence of protein are related to motor neuron impairment.[6,7]

Following processes accompanied by neural damage, NF-L is released in significant amounts into the interstitial fluid and eventually into the cerebrospinal fluid (CSF) and blood, reaching abnormal levels. Therefore, CSF and blood NF-L levels could be used as a direct marker of neuronal damage, providing an indication of axonal injury, axonal loss, and neuronal death.[1,4]

K. Solodka, M. Berto, C. A. Bortolotti, F. Biscarini, M. Pinti
Department of Life Sciences
University of Modena and Reggio Emilia
Via Campi 103, Modena 41125, Italy
E-mail: carloaugusto.bortolotti@unimore.it;
marcello.pinti@unimore.it

The ORCID identification number(s) for the author(s) of this article can be found under https://doi.org/10.1002/admi.202102341.

DOI: 10.1002/admi.202102341

D. Ferraro
Department of Biomedical
Metabolic and Neural Sciences
University of Modena and Reggio Emilia
Via Campi 287, Modena 41125, Italy

C. Menozzi
Department of Physics
Informatics and Mathematics
University of Modena and Reggio Emilia
Via Campi 213/a, Modena 41125, Italy

M. Borsari
Department of Chemical and Geological Sciences
University of Modena and Reggio Emilia
Via Campi 103, Modena 41125, Italy

F. Biscarini
Istituto Italiano di Tecnologia – Center for Translational Neurophysiology
Via Fossato di Mortara 17–19, Ferrara 44121, Italy

MS is a chronic inflammatory disorder of the central nervous system (CNS), characterized by progressive axonal demyelination and neurodegeneration.[8] The prevalence of MS has increased over the last years, and to date, it is estimated that 2.8 million people suffer from this disease worldwide. Because of its high prevalence, MS is considered as the major cause of nontraumatic neurologic disability in young adults.[9]

The etiology of MS is still unknown, and both genetic susceptibility and environmental factors play a key role in the development of the disease. Although the precise mechanism of disease initiation is not yet completely understood, it is presumed to be an autoimmune disease, with inflammation acting as the driving force for disease development.[8,10] The initiation of the disease comprises the activation of peripheral immune cells and their progressive infiltration into the CNS across the blood–brain barrier, which leads to inflammation, demyelination, and finally, neuroaxonal damage, which triggers the disruption of neuronal signaling.[10,11]

The pathology of MS is highly heterogeneous in terms of clinical presentation, pathological phenotypes, disease progression, and treatment response,[12,13] which makes the assessment of an early and proper diagnosis very challenging. Furthermore, many neuroinflammatory disorders, such as neuromyelitis optica spectrum disorders (NMOSD), present similar features,[14] which is an additional difficulty.

Currently, the most extensively used tools in the diagnosis and monitoring of MS patients are magnetic resonance imaging (MRI) and CSF analysis.[15] The detection of white matter lesions in the CNS by MRI provides valuable information on the anatomical and temporal dissemination of areas of demyelination. Because of its high sensitivity and specificity for lesion detection and dissemination, MRI can be used for monitoring disease activity and prognostic evaluation, as well as an assessment tool of treatment response.[16,17] CSF analysis is a useful tool to support the diagnosis of MS, and it can provide additional information regarding inflammation and immunological status of the patient. The presence of oligoclonal bands in CSF and an elevated IgG index are typical features in MS patients.[18] Additionally, because MS is presumed to have an inflammatory origin, the level of many proinflammatory mediators, such as IL-6, TNF-α, IFN-γ, and CXCL13, is increased in the CSF of MS patients.[19–21] Although these parameters may have a diagnostic and prognostic value, they are not specific to MS and can be also found in a variety of neurological diseases.[22–24] Therefore, there is an urgent need for new biomarkers to critically differentiate MS from other demyelinating disorders in order to assess an early and accurate diagnosis, as well as for monitoring disease activity and treatment response.

Recent studies reported increased levels of NF-L in plasma or serum of MS patients, which correlated with patient disability, disease activity, brain atrophy, and spinal cord volume loss.[25–32] Interestingly, it was also observed that the levels of NF-L were elevated even when no focal inflammatory MRI activity was detected,[25] and following disease-modifying therapies, NF-L levels decreased in CSF and serum.[30,33] This evidence supports the potential value of NF-L as a biomarker for neural damage and an important element for early MS prognosis.

Initially, the detection of NF-L was based on the analysis of CSF using enzyme-linked immunosorbent assays and electrochemiluminescence-based assays. However, since obtaining CSF is an invasive procedure, blood has become the sample of choice for NF-L detection. Because the levels of NF-L in serum and plasma are considerably lower than in CSF, these methods present a relatively low sensitivity. Nowadays, single-molecule array represents the state-of-the-art technique for NF-L detection in biological fluids.[34] Although this assay is highly sensitive and specific, it presents some limitations: it is time consuming, needs specialized equipment, and a dedicated laboratory with trained personnel, as well as fluorescent or enzymatic labeling for detection.

Thanks to the recent progress in material design and device architectures, organic bioelectronic devices have been demonstrated in a number of brand-new applications, such as high-sensitive pressure sensing, soft bioelectronics, and robotics.[35–38] Among them, electrolyte-gated organic field-effect transistors (EGOFETs), are emerging as a highly versatile biosensing platform alternative to (or at least complementing) optical assays: thus far, EGOFETs have been explored for biosensing of clinically and environmentally relevant molecules such as nucleic acids,[39–41] inflammatory cytokines,[42–44] antidrug antibodies,[45] and even viruses.[46] EGOFETs are three-electrode devices, with source and drain bridged by an organic semiconductor (OSC) layer, which is separated from the third electrode, the gate, by an electrolyte that replaces conventional dielectric. Upon application of a potential between gate and source (V_{GS}), gating is achieved by electrolyte ions forming electrical double layers at the gate/electrolyte and electrolyte/OSC interfaces, the latter causing accumulation of charge carriers (holes, in the case of p-type semiconductors as in the present work) in the OSC that can give rise to a current flowing between the source and drain upon application of a second potential V_{DS}. EGOFETs can be operated as biosensors upon integration of a specific recognition moiety (e.g., an antibody or an aptamer) at one of the device interfaces. Functionalization of the gate (typically made of Au) is often preferred, as it allows to exploit a wide portfolio of surface modification strategies to achieve immobilization of the specific recognition moiety, still enabling the detection of biorecognition events (such as antigen/antibody interaction) through changes in the source–drain current thanks to the capacitive coupling.

Here, we show the first EGOFET immunosensor able to detect NF-L down to sub-pM concentrations with high specificity, which is achieved by immobilization of anti-NF-L antibodies on the device gate electrode. In particular, we validated the biosensor for detecting NF-L in buffered solutions at physiological pH with a focus on the reproducibility of the device response, by performing a large number ($n = 11$) of independent experiments. Moreover, we thoroughly assessed the capability to selectively detect NF-L by a set of control experiments where we changed either the specific recognition unit or the target or even by obtaining a full dose curve in the presence of a potentially interfering cytokine. Our results hint at the fact that EGOFETs can serve as label-free biosensors for the detection of NF-L in physio-pathological ranges.

2. Results and Discussion

2.1. Gate Functionalization with NF-L-Specific Recognition Elements

The schematics of the NF-L biosensor developed in this study are depicted in **Figure 1**. The device is based on the EGOFET

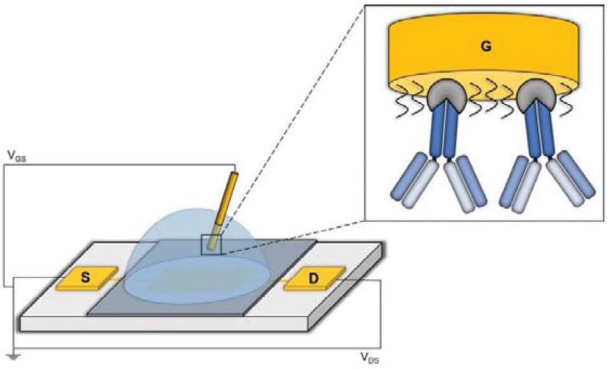

Figure 1. Schematics of the EGOFET-based biosensor, including source, drain, and gate electrodes, and electrical connections. In order to mimic physiological conditions, all electrical measurements were carried out using PBS as electrolyte solution. The inset shows the functionalization process used in this study. Anti-NF-L antibodies have been noncovalently bound to the gate exploiting the affinity of their Fc fragment for cys-Protein G previously adsorbed on the Au surface, which is further passivated with an OEG SAM.

architecture, with a top gate electrode endowed with sensing capability through immobilization of anti-NF-L antibodies on the gate electrode with controlled orientation. The latter is sought through the formation of a (sub)monolayer primer of Protein G, covalently bound to the bare gold gate through the presence of a single solvent-exposed Cys residue. The use of a Protein G (sub) monolayer to control the antibody orientation has been previously explored by our group to endow EGOFET gate electrodes with selectivity toward proteins and viruses.[45–47] Following this first step, the high affinity of Protein G for the fragment crystallizable (Fc) regions of the heavy chains of immunoglobulins G allowed the immobilization of antibodies with a definite and potentially uniform orientation. The last functionalization step consisted of the formation of an OEG self-assembled monolayer (SAM): OEG SAMs have been proven to exhibit antifouling properties,[48] and we, therefore, introduced this last passivation step in an attempt to reduce nonspecific binding.

The gate functionalization process was monitored by electrochemical and electrical characterization. During the former, cyclic voltammetry (CV) experiments in the presence of 5 mM $K_3[Fe(CN)_6]$ in 1 M KCl were performed. As expected, the immobilization of Protein G led to an increase in the peak-to-peak separation, hinting at the successful adsorption onto Au (Figure S1A, Supporting Information). The subsequent immobilization of the antibody did not cause significant changes in the CV curves. A drastic change is instead observed after the SAM formation, which leads to complete inhibition of the faradaic response, indicating a total coverage of the Au gold surface. From these measurements, the covered area of the electrode by Protein G-antibody was calculated by means of the Randles–Ševçik equation and was estimated to be 40 ± 4%. In parallel, the gate functionalization was also monitored by electrical characterization, and in particular by obtaining transfer curves of EGOFETs gated by an Au gate electrode following each modification step. The overlay of the transfer characteristics recorded after each functionalization step showed a decrease in the drain current following every modification of the Au surface (Figure S1B, Supporting Information). Fabrication and functionalization protocols showed good reproducibility: typical transfer curves and output characteristics registered with bare Au gate electrode and Protein G/NF-L antibody/OEG SAM functionalized gate electrode are reported in Figure S2, Supporting Information. The devices showed good electrical performances even after the gate functionalization; in particular, transconductance g_m, that is, the slope of the linear region of the transfer curves, slightly decreases from g_m = 2.2 (± 0.7) μS to 2.0 (± 0.6) μS moving from bare gold gate to functionalized gate, respectively. The gate functionalization protocol caused a shift of the threshold voltage V_{TH} to more negative values, from V_{TH} = –0.31 (± 0.04) V to –0.38 (± 0.03) V, and an increase of the ON/OFF current ratio from ≈1000 to ≈3000. The increase is due to the lowering of the OFF current, probably caused by a decrease of leakage current I_{GS} after the functionalization steps. The output characteristics reported in Figure S2, Supporting Information show a good modulation of the drain current I_{DS} (the saturation region is reached at V_{DS} between –0.2 and –0.3 V).

2.2. Sensing NF-L with EGOFET-Based Biosensors

After assessing the effectiveness of the gate functionalization strategies, we tested the capability of EGOFETs gated by the cys-Protein G/anti-NF-L/OEG-modified Au electrodes to serve as biosensors selective toward NF-L in a concentration range that would span both physiological and pathological levels.[27,29] To this end, we first recorded transfer characteristics in the –0.1 to –0.6 V potential window in PBS containing increasing concentrations of NF-L ranging from 100 fM to 10 nM. **Figure 2**A displays a typical response of EGOFETs to increasing [NF-L]: the drain current invariably decreases as the target protein concentration increases. We ascribe the [NF-L]-dependent change of the drain current to NF-L binding to the corresponding antibody immobilized on the gate. The sensor gives a response in a few minutes and shows good stability in time as reported in Figure S3, Supporting Information for 10 pM [NF-L] solution. In line with previous reports by our group and others,[40,47,49–51] we quantify the response of the biosensor as $-\Delta I/I_0 = -(I_{DS(n)} - I_{DS(0)})/I_{DS(0)}$, where $I_{DS(n)}$ is the drain current value at the nth NF-L concentration, and $I_{DS(0)}$ is the drain current value at [NF-L] = 0 M. $-\Delta I/I_0$ can be calculated at any V_{GS} value explored while recording the transfer curve. It has been previously shown that the normalized drain current change $\Delta I/I_0$ is typically highest for V_{GS} values below or close to the threshold voltage V_{TH}. Therefore, here we decide to focus on the dose curve calculated at V_{GS} = –0.4 V, depicted in Figure 2B in the semilogarithmic format.

$-\Delta I/I_0$ increases monotonically within the investigated [NF-L] range: it rises rapidly at the lowest concentrations tested (i.e., for [NF-L] ≤ 10 pM), then it still increases but in a less steep way to reach [NF-L] = 1 nM and eventually rises rapidly again until the highest concentration tested [NF-L] = 10 nM is reached. At a first glance, this trend hints at the concomitant presence of two simultaneous equilibria taking place at the gate/electrolyte interface. To gain insight into the experimentally observed trend of $-\Delta I/I_0$ versus [NF-L], we fitted the corresponding dose curve with the liquid phase version of the Guggenheim–Anderson–De Boer (GAB) adsorption model. The GAB isotherm is a

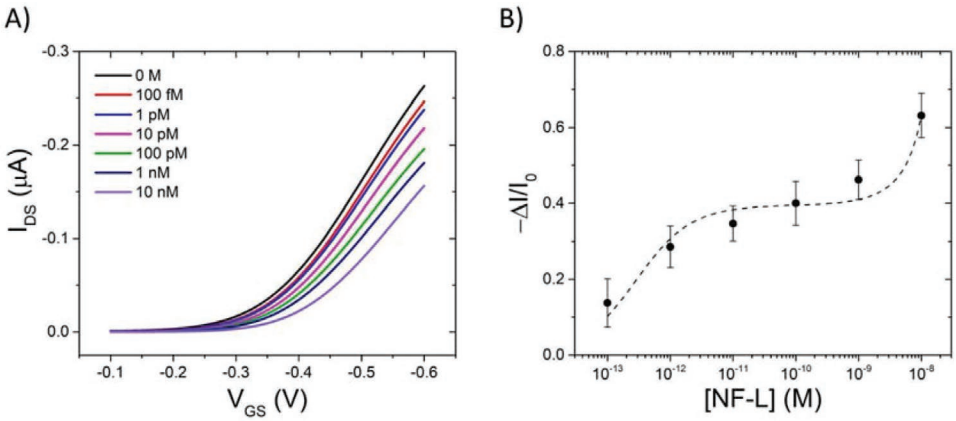

Figure 2. Transfer characteristics and response of the device to NF-L. A) Transfer curves of the EGOFET-based biosensor upon exposure to increasing concentrations of NF-L in PBS, ranging from 100 fM to 10 nM, recorded at a fixed V_{DS} of –0.2 V. This is a representative example of the 11 experiments performed; the highest concentration (10 nM) was tested in 8 out of 11 replicates, while the lowest (100 fM) in 3. B) Biosensor dose curve $-\Delta I/I_0$ versus log[NF-L], calculated at V_{GS} = –0.4 V. Data are shown as the mean ± SE of 11 independent experiments. Dashed line is the fit to the GAB adsorption isotherm (Equation 1).

three-parameter, multilayer adsorption model that is based on the assumption of two distinct adsorption states: a first layer is characterized by strong adsorption and is associated to an equilibrium constant K_S, whereas the binding of more adsorbate molecules to form a second (or multiple) layer(s), in a different state than those in the first adlayer, is weaker and described by a second equilibrium constant K_L. This second layer generally forms on the previous layer strongly adsorbed on the adsorbent surface.

The GAB model has been applied to the description of protein adsorption on silica nanoparticles.[52,53] Here, we apply it to the problem of NF-L binding to EGOFET gates by expressing the isotherm in terms of $-\Delta I/I_0$ (which we assume is directly proportional to the amount of adsorbed NF-L) as follows

$$\frac{\Delta I}{I_0} = \left(\frac{\Delta I}{I_0}\right)_{max} \frac{K_S C}{(1-K_L C)(1+K_S C-K_L C)} \quad (1)$$

where $(-\Delta I/I_0)_{max}$ is the maximum attainable normalized drain current change upon adsorption in the first strongly bound layer (therefore directly proportional to the maximum surface concentration of NF-L) and C is the bulk protein concentration. Please note that $-\Delta I/I_0$ will take values > $(-\Delta I/I_0)_{max}$ if $K_L > 0$ (therefore, if multilayers are formed), since $(-\Delta I/I_0)_{max}$ is related to the maximum amount of protein adsorbed exclusively in the first, strongly bound layer; if, instead, $K_L = 0$, there is no multilayer formation and the GAB isotherm is reduced to the Langmuir model. The dashed line in Figure 2B is the fit of the GAB isotherm to our data, with the best-fit parameters taking the following values: $K_S = (3.52 \pm 1.63) \times 10^{12}$, $K_L = (3.78 \pm 0.54) \times 10^7$ and $(\Delta I/I_0)_{max} = 0.39 \pm 0.02$. The GAB model seems to fit rather well with our experimental data. The satisfactory fitting indicates that the Langmuir-like treatment of the strong adsorption state, which does not take into account lateral interactions between antibody/NF-L couples, describes reasonably well our experimental conditions also in line with the estimated protein G coverage of the gate electrode. Three regions can be identified in Figure 2B that correspond to lowest, intermediate, and highest [NF-L] values, respectively. Within the framework provided by the GAB isotherm, these regions can be associated with two adsorption processes that partly overlap. At low concentrations of NF-L protein in solution, there is a progressive increase in the surface concentration of protein strongly bound to the surface-confined antibody; when this first adsorption process approaches saturation (region of pseudo-plateau), a second adsorption process begins on low-affinity sites, most likely corresponding to binding from solution to antibody-bound NF-L molecules resulting in multilayers of NF on the electrode surface. This second adsorption process yields the third region, characterized by a rapid increase in the amount of adsorbed protein which is observed when the high-affinity sites are saturated, and the adsorption occurs only on the low-affinity sites. Processes of this type, described by a GAB isotherm where a second adsorption process occurs on the first layer of adsorbed protein, are known in the literature.[52–54] The possibility that the protein/protein aggregation might be occurring on the surface was considered, also taking into account the demonstrated ability of NFs, including (though not limited to) NF-L, to assembly in vitro and in vivo.[55–59]

Fitting with the GAB isotherm also allowed us to estimate the limit of detection (LOD), namely the concentration corresponding to the device signal when no analyte is present in the measurement environment + 3σ (σ is the standard deviation of the device response). In this case, the LOD is as low as 30 fM.

2.3. Morphological Characterization

To assess whether high concentrations of NF-L might indeed lead to the formation of aggregates on the gate surface, we performed semicontact atomic force microscopy (AFM) imaging in air on cys-Protein G/anti-NF-L/OEG-modified Au electrodes before and after immersion in NF-L solutions at increasing concentration. AFM images recorded at [NF-L] = 0 M, 1 pM, 100 pM, and 10 nM are shown in **Figure 3**. It is apparent that the

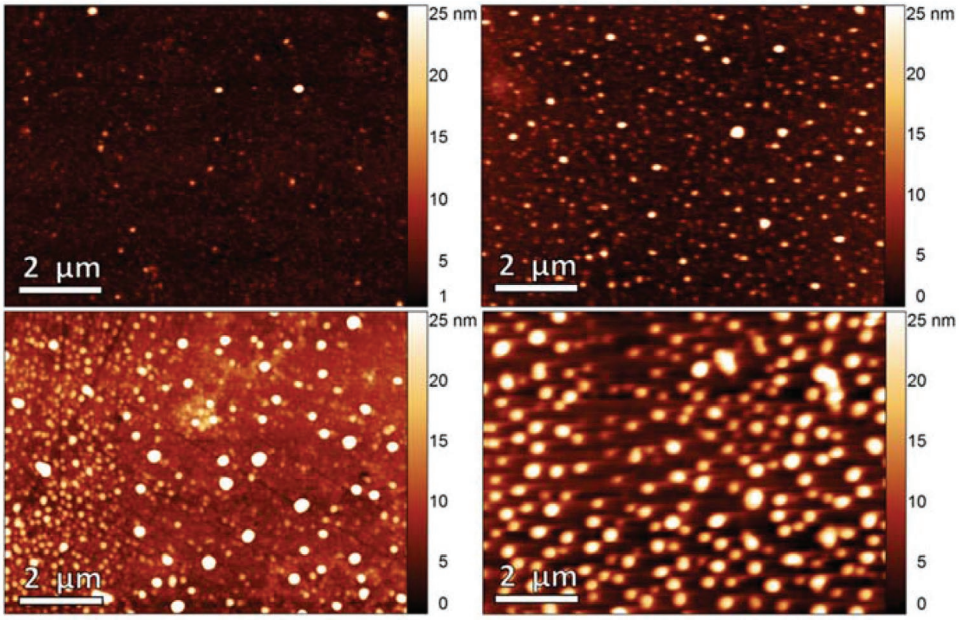

Figure 3. AFM topographical images of cys-Protein G/anti-NF-L/OEG-modified Au electrodes after immersion in NF-L containing solution at increasing concentration: 0 M (top left), 1 PM (top right), 100 PM (bottom left), and 10 NM (bottom right).

morphology of the gate electrodes is heavily dependent on [NF-L]. One can note rounded morphological features that we can safely describe as NF-L-related entities, whose heights are in tens of NM range, whose density increases with increasing NF-L concentration, and that, therefore, might be tentatively interpreted as protein aggregates. The NF-L concentration-related morphology has been confirmed by scanning electron microscopy (SEM) analysis of the same electrodes (Figure S4, Supporting Information). Interestingly, the NF-L aggregates show a globular shape, thus different from the elongated shapes previously described when NF-L is associated with NF-M and NF-H.[58,60,61] To quantitatively describe the morphological surface changes with [NF-L], we estimated the average surface roughness σ_{rms} and the correlation length ξ, which are reported in Table S1, Supporting Information (standard deviations from different images of the same electrode are reported as errors). The immobilization of NF-L causes a monotonic increase of the surface roughness moving from 1 PM to 10 NM due to the increasing number and dimension of protein aggregates.

Conversely, the lateral correlation length decreases with increasing NF-L concentration since the distances between the aggregates decrease. Both trends corroborate our interpretation that NF-L aggregation might take place on the gate at high concentrations.

2.4. Evaluation of Selectivity of NF-L Sensor

In order to assess whether the observed device response could be safely ascribed to selective interaction between NF-L and its corresponding antibody immobilized on the Au gate electrode, we performed the following set of control experiments. First, we monitored the response of EGOFETs gated by Au electrodes with anti-interleukin-6 (IL-6) antibodies, instead of anti-NF-L ones, immobilized on the electrode surface. In such a configuration, no biorecognition unit specific to NF-L is present on the gate surface; therefore, we expected ideally no specific response upon exposure to increasing [NF-L] in solution. In **Figure 4**A, we provide the response to the highest NF-L concentration (10 NM) tested with EGOFETs gated by cys-Protein G/anti-IL-6/OEG-modified Au electrodes. It is apparent that, despite the rather large error bar associated with the average $-\Delta I/I_0$ value, the nonspecific response is significantly lower even than the specific response, averaged over 11 different experiments, to 1 NM NF-L (therefore, 10 times less concentrated). The response of EGOFETs gated by cys-Protein G/anti-IL-6/OEG-modified Au electrodes to lower NF-L concentration (1 PM to 1 NM) is even smaller in magnitude and opposite in sign with respect to the specific one (data not shown). These results indicate that the trend observed in Figure 2A requires, as expected, the presence of a specific biorecognition unit on the gate.

In the second round of control experiments, we monitored the response of EGOFETs gated by Au electrodes with anti-NF-L antibodies to biomacromolecules different from NF-L. For this purpose, we exposed the biosensor to other proteins, which might in principle bind nonspecifically at the relevant device interfaces yielding an undesired nonspecific response. We tested two inflammatory cytokines normally present in the same fluids where NF-L can be found, namely IL-6 and IL-1β. The response to a high (10 NM) concentration of inflammatory cytokines was evaluated in triplicate (Figure 4A). Please note that we chose to test interleukin concentrations that are well above the physiological (about 0.05 PM) and pathological (about 0.05 NM) levels. It is apparent that both cytokines caused a nonspecific response that is markedly lower than the specific one, even when compared with the response to 1 NM NF-L.

Finally, we checked if the sensitivity of the biosensor would be influenced by the presence of other, potentially interfering

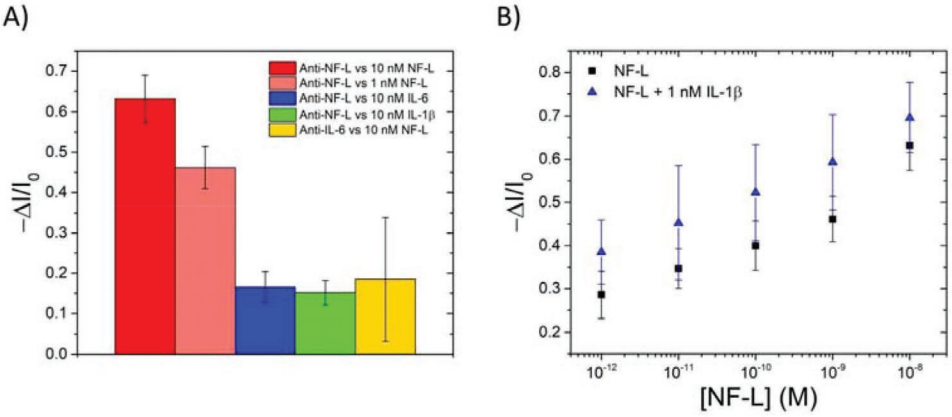

Figure 4. A) Response of the EGOFET-based biosensor functionalized with either specific anti-NF-L antibodies to different proteins: NF-L (red), IL-6 (blue), and IL-1β (green), or with anti-IL-6 antibodies to NF-L (yellow). Data are shown as mean ± SE of 11 (red) and 3 (blue, green, and yellow) independent experiments. B) Biosensor dose curve $-\Delta I/I_0$ versus molar concentration of NF-L, in the absence (black squares) and presence (blue triangles) of 1 nM IL-1β, calculated at $V_{GS} = -0.4$ V. Data are shown as mean ± SE of 11 (black squares) and 4 (blue triangles) independent experiments.

molecules. We, therefore, tested the response of EGOFET gated by Au electrodes with immobilized anti-NF-L antibodies to increasing [NF-L] in the presence of a potentially interfering molecule, IL-1β, at a constant, high concentration (1 nM). This last set of experiments was repeated in quadruplicate, and the results are shown in Figure 4B, with data points as blue triangles, overlaid to the corresponding dose curve in the same [NF-L] range but in the absence of IL-1β (black squares). Although, at all tested concentrations, the response to the target is slightly higher than that in the absence of IL-1β, the current variations are indistinguishable when considering the associated errors. Therefore, even in the presence of a potentially interfering protein, the device was still able to discriminate NF-L in the 10 pM–10 nM range.

Overall, these three rounds of control experiments all indicate that our device is able to selectively discriminate NF-L in the investigated concentration range.

3. Conclusions

In summary, we demonstrated successful detection of NF-L with an EGOFET biosensor. The biosensor developed in this study turned out to be able to detect NF-L in a dynamic range spanning five orders of magnitude, from 100 fM to 10 nM, with satisfactory reproducibility that was assessed by the large number of independent experiments performed.

The data distribution along the dose curve hinted at the simultaneous presence of at least two equilibria: along this line, the device response was fitted to the GAB isotherm, which takes into account multilayer adsorption. We interpret successful fitting to the GAB model in terms of formation of a strongly bound layer where antibody/antigen interaction takes place, and we hypothesize that further layers might be formed upon NF-L aggregation on the gate surface, as indirectly supported also by AFM investigations on gold surfaces functionalized like the EGOFET gates and exposed to increasing [NF-L].

We assessed the selectivity of the biosensors for NF-L, by evaluating the nonspecific response when either the surface probe (the antibody) or the target (the freely diffusing protein) was changed. In both cases, the specific response was significantly higher. Further confirmation of selectivity came from the dose curve obtained in the presence of a second, potentially interfering protein at a high, constant concentration.

We are well aware that further optimization of the biosensor is needed before applying it to the quantification of NF-L in biological samples. In particular, validation with highly complex media such as serum and plasma will have to be performed, to check whether the selectivity is retained also when operated in bodily fluids, a matter that might be relevant especially considering the low NF-L concentrations (i.e., $<10^{-11}$ M), typically observed in real samples. Nevertheless, we believe that the present data make our sensing platform a highly promising candidate to monitor the progression of multiple sclerosis and possibly also the response to treatment.

4. Experimental Section

Device Fabrication: The transistors were fabricated using test patterns (TPs) of 1 cm^{-2} total area purchased from "Fondazione Bruno Kessler" (Trento, Italy). TPs presented four interdigitated source and drain electrodes with a channel length L = 15 µm and channel width W = 30 mm (W/L = 2000) patterned by photolithography and lift-off. Source and drain electrodes were made of Au with a thickness of 50 nm and a few nm Cr adhesive layer on a quartz substrate. Prior to the semiconductor deposition, TPs were cleaned as follows: i) removal of the photoresist layer by rinsing with acetone, ii) drying with nitrogen flow, iii) washing in acetone at 70 °C for 10 min, iv) drying with nitrogen flow, v) immersion in piranha solution (1:1 concentrated H_2SO_4:H_2O_2) at 150 °C for 1 min, vi) abundant rinsing with water, vii) drying with nitrogen flow. TIPS-pentacene (2% w/w in 80:20 toluene:hexane) was deposited on the quartz substrate by spin coating and cured in a solvent-rich environment at 60 °C for 30 min.

Gate Functionalization: Polycrystalline gold wires were used as gate electrodes. Prior to functionalization, gold wires were cleaned through i) immersion in 2.5 M KOH at 130 °C for 4 h, ii) immersion in concentrated H_2SO_4 at 220 °C for 2 h, iii) rinse abundantly with water. A final electrochemical polish was performed by sweeping the potential between 1.5 and –0.25 V in acidic conditions (1 M H_2SO_4) for at least five cycles.

Specific recognition elements were immobilized in the gate surface according to the following protocol: i) overnight incubation in cys-Protein G solution (2 mg mL^{-1}) at 4 °C, ii) incubation in anti-NF-L solution (0.1 mg mL^{-1}) for 1 h at room temperature, iii) incubation in 11-mercaptoundecyl-triethylene glycol (OEG) solution (10 µM) for 30 min at room temperature, iv) final rinse with PBS. The area of the gold electrodes was kept constant by means of a passivation layer.

Electrochemical Characterization: Cyclic voltammetry (CV) measurements were performed to estimate the electrode active area and the coverage after every immobilization step by means of the Randles–Ševçik equation. The measurements were performed in 5 mM $K_3[Fe(CN)_6]$, 1 M KCl at 50 mV s^{-1}. The experiments were carried out using a CH Instrument potentiostat 760c model. All measurements were performed in a three-electrode cell; the Au gate electrode was used as the working electrode, whereas Pt and Ag/AgCl electrodes were used as counter and reference electrodes, respectively.

Electrical Characterization: Electrical measurements were acquired in a buffer solution (50 mM PBS, pH 7.4) containing increasing concentrations of NF-L (from 100 fM to 10 nM). Source, drain, and gate electrodes were connected to an Agilent B2912A Source Measure Unit, and current–voltage (*I*–*V*) characteristics were recorded by applying sweeping gate–source voltage (V_{GS}) from −0.1 to −0.6 V while maintaining a constant drain–source voltage (V_{DS}) of −0.2 V. All the measurements were performed at room temperature inside a Faraday cage. Transfer curves were repeatedly acquired until reaching stabilization. The experimental values shown in Figure 2 are the average of the measurements performed for $n = 11$ experiments, except for [NF-L] = 10 nM and [NF-L] = 100 fM, for which $n = 8$ and $n = 3$, respectively. Error bars represent the associated standard error (SE) of the mean.

Control Experiments: In the first set of control experiments ($n = 3$), the EGOFET gate was functionalized following the same procedure as described previously but immobilizing anti-IL-6 antibodies instead of anti-NF-L ones. In the second set of control experiments ($n = 3$), the gate was functionalized exactly as described previously and the device was exposed to 50 mM PBS, pH 7.4 solutions containing IL-6 or IL-1β at 1 and 10 nM concentrations. In the third set of control experiments, ($n = 4$), the gate was functionalized exactly as described previously and the device was exposed to 50 mM PBS, pH 7.4 solutions containing increasing concentrations of NF-L in the 1 pM–10 nM range together with 1 nM IL-1β. The experiments were performed under the same conditions as the sensing experiments described above.

Atomic Force Microscopy: Morphological characterization of the electrodes was performed using an NT-MDT SMENA Solver platform (Moscow, Russia); the analysis has been performed in semicontact mode and the images have been analyzed using Gwyddion 2.56 freeware (http://gwyddion.net). The electrode characterized with AFM was different from the one used in electrical measurements; in particular, a flat electrode was used to optimize the morphological analysis (fabrication and cleaning procedures are reported in ref. [39]).

Scanning Electron Microscopy: Surface characterization was performed with a SEM Zeiss Sigma equipped with a Schottky Field Emission Gun operating at 5 keV.

Chemicals and Reagents: Phosphate salts, potassium ferricyanide, potassium chloride, sulfuric acid, potassium hydroxide, acetone, acetone, ethanol, hexane, toluene, and OEG were purchased from Sigma-Aldrich. TIPS-pentacene was purchased from Ossila. Cys-Protein G was purchased from Novus Biologicals. Monoclonal anti-NF-L (DA2) and anti-IL-6 (677B6A2) antibodies were purchased from Thermo Fisher Scientific. Recombinant human NF-L, IL-6, and IL-1β proteins were purchased from Abcam, ReliaTech GmbH, and AdipoGen, respectively.

Supporting Information

Supporting Information is available from the Wiley Online Library or from the author.

Acknowledgements

This project received funding from the European Union's Horizon 2020 research and innovation programme under the Marie Sklodowska-Curie grant agreement no. 813863.

Conflict of Interest

The authors declare no conflict of interest.

Data Availability Statement

The data that support the findings of this study are openly available in Zenodo at https://doi.org/10.5281/zenodo.5821640, reference number 5821640.

Keywords

electrolyte-gated organic field-effect transistors, Guggenheim–Anderson–De Boer isotherm, multiple sclerosis, neurofilament light chain

Received: November 29, 2021
Revised: January 13, 2022
Published online: February 10, 2022

[1] M. Khalil, C. E. Teunissen, M. Otto, F. Piehl, M. P. Sormani, T. Gattringer, C. Barro, L. Kappos, M. Comabella, F. Fazekas, *Nat. Rev. Neurol.* **2018**, *14*, 577.
[2] K. L. Lambertsen, C. B. Soares, D. Gaist, H. H. Nielsen, *Brain Sci.* **2020**, *10*, 56.
[3] N. J. Cairns, V. M. Lee, J. Q. Trojanowski, *J. Pathol. A J. Pathol. Soc* **2004**, *204*, 438.
[4] A. Yuan, M. V. Rao, R. A. Nixon, *Cold Spring Harb. Perspect. Biol.* **2017**, *9*, a018309.
[5] Q. Liu, F. Xie, S. L. Siedlak, A. Nunomura, K. Honda, P. I. Moreira, X. Zhua, M. A. Smith, G. Perry, *Cell. Mol. Life Sci.* **2004**, *61*, 3057.
[6] M. T. Sainio, E. Ylikallio, L. Mäenpää, J. Lahtela, P. Mattila, M. Auranen, J. Palmio, H. Tyynismaa, *Neurol. Genet.* **2018**, *4*.
[7] J. Zhai, H. Lin, J.-P. Julien, W. W. Schlaepfer, *Hum. Mol. Genet.* **2007**, *16*, 3103.
[8] H. Lassmann, W. Brück, C. F. Lucchinetti, *Brain Pathol.* **2007**, *17*, 210.
[9] https://www.atlasofms.org/map/global/epidemiology/number-of-people-with-ms, (accessed: November 2021).
[10] C. A. Dendrou, L. Fugger, M. A. Friese, *Nat. Rev. Immunol.* **2015**, *15*, 545.
[11] R. Dutta, B. D. Trapp, *Neurology* **2007**, *68*, S22.
[12] H. Lassmann, W. Brück, C. Lucchinetti, *Trends Mol. Med.* **2001**, *7*, 115.
[13] F. D. Lublin, S. C. Reingold, J. A. Cohen, G. R. Cutter, P. S. Sørensen, A. J. Thompson, J. S. Wolinsky, L. J. Balcer, B. Banwell, F. Barkhof, *Neurology* **2014**, *83*, 278.
[14] C. Eckstein, S. Saidha, M. Levy, *J. Neurol.* **2012**, *259*, 801.
[15] W. J. Housley, D. Pitt, D. A. Hafler, *Clin. Immunol.* **2015**, *161*, 51.
[16] M. Filippi, P. Preziosa, M. A. Rocca, *Curr. Opin. Neurol.* **2018**, *31*, 386.
[17] A. Giorgio, N. De Stefano, *Neurol. Clin* **2017**, *36*, 27.
[18] M. Stangel, S. Fredrikson, E. Meinl, A. Petzold, O. Stüve, H. Tumani, *Nat. Rev. Neurol.* **2013**, *9*, 267.

[19] M. S. Bassi, E. Iezzi, F. Mori, I. Simonelli, L. Gilio, F. Buttari, F. Sica, N. De Paolis, G. Mandolesi, A. Musella, *Neurorehabil. Neural Repair* **2019**, *33*, 825.
[20] D. Ferraro, V. Galli, F. Vitetta, A. M. Simone, R. Bedin, C. Del Giovane, F. Morselli, M. M. Filippini, P. F. Nichelli, P. Sola, *J. Neuroimmunol.* **2015**, *283*, 64.
[21] R. Magliozzi, A. Scalfari, A. I. Pisani, S. Ziccardi, D. Marastoni, F. B. Pizzini, A. Bajrami, A. Tamanti, M. Guandalini, S. Bonomi, *Ann. Neurol.* **2020**, *88*, 562.
[22] J. C. Janssen, A. K. Godbolt, P. Ioannidis, E. J. Thompson, M. N. Rossor, *J. Neurol.* **2004**, *251*, 184.
[23] E. Alvarez, L. Piccio, R. J. Mikesell, E. C. Klawiter, B. J. Parks, R. T. Naismith, A. H. Cross, *Mult. Scler. J.* **2013**, *19*, 1204.
[24] X. Chen, Y. Hu, Z. Cao, Q. Liu, Y. Cheng, *Front. Immunol.* **2018**, *9*, 2122.
[25] C. Barro, P. Benkert, G. Disanto, C. Tsagkas, M. Amann, Y. Naegelin, D. Leppert, C. Gobbi, C. Granziera, Ö. Yaldizli, *Brain* **2018**, *141*, 2382.
[26] D. Ferraro, C. Guicciardi, S. De Biasi, M. Pinti, R. Bedin, V. Camera, F. Vitetta, M. Nasi, S. Meletti, P. Sola, *Acta Neurol. Scand.* **2020**, *141*, 16.
[27] G. Disanto, C. Barro, P. Benkert, Y. Naegelin, S. Schädelin, A. Giardiello, C. Zecca, K. Blennow, H. Zetterberg, D. Leppert, *Ann. Neurol.* **2017**, *81*, 857.
[28] I. Håkansson, A. Tisell, P. Cassel, K. Blennow, H. Zetterberg, P. Lundberg, C. Dahle, M. Vrethem, J. Ernerudh, *J. Neuroinflammation* **2018**, *15*, 209.
[29] L. Novakova, H. Zetterberg, P. Sundström, M. Axelsson, M. Khademi, M. Gunnarsson, C. Malmeström, A. Svenningsson, T. Olsson, F. Piehl, *Neurology* **2017**, *89*, 2230.
[30] J. Kuhle, H. Kropshofer, D. A. Haering, U. Kundu, R. Meinert, C. Barro, F. Dahlke, D. Tomic, D. Leppert, L. Kappos, *Neurology* **2019**, *92*, e1007.
[31] I. Håkansson, A. Tisell, P. Cassel, K. Blennow, H. Zetterberg, P. Lundberg, C. Dahle, M. Vrethem, J. Ernerudh, *Eur. J. Neurol.* **2017**, *24*, 703.
[32] T. Uher, S. Schaedelin, B. Srpova, C. Barro, N. Bergsland, M. Dwyer, M. Tyblova, K. Vodehnalova, P. Benkert, J. Oechtering, *Neurol. Neuroinflammation* **2020**, *7*.
[33] T. Sejbaek, H. H. Nielsen, N. Penner, T. Plavina, J. P. Mendoza, N. A. Martin, M. L. Elkjaer, M. H. Ravnborg, Z. Illes, *J. Neurol. Neurosurg. Psychiatry* **2019**, *90*, 1324.
[34] J. Kuhle, C. Barro, U. Andreasson, T. Derfuss, R. Lindberg, Å. Sandelius, V. Liman, N. Norgren, K. Blennow, H. Zetterberg, *Clin. Chem. Lab. Med.* **2016**, *54*, 1655.
[35] Z. Yin, M. J. Yin, Z. Liu, Y. Zhang, A. P. Zhang, Q. Zheng, *Adv. Sci.* **2018**, *5*, 1701041.
[36] C. F. Guo, L. Ding, *Innov.* **2021**, *2*, 100074.
[37] I. Krauhausen, D. A. Koutsouras, A. Melianas, S. T. Keene, K. Lieberth, H. Ledanseur, R. Sheelamanthula, A. Giovannitti, F. Torricelli, I. McCulloch, P. W. M. Blom, A. Salleo, Y. van de Burgt, P. Gkoupidenis, *Sci. Adv.* **2021**, *7*, eabl5068.
[38] F. Torricelli, D. Z. Adrahtas, Z. Bao, M. Berggren, F. Biscarini, A. Bonfiglio, C. A. Bortolotti, C. D. Frisbie, E. Macchia, G. G. Malliaras, I. McCulloch, M. Moser, T.-Q. Nguyen, R. M. Owens, A. Salleo, A. Spanu, L. Torsi, *Nat. Rev. Methods Prim.* **2021**, *1*, 66.
[39] M. Selvaraj, P. Greco, M. Sensi, G. D. Saygin, N. Bellassai, R. D'Agata, G. Spoto, F. Biscarini, *Biosens. Bioelectron.* **2021**, *182*, 113144.
[40] E. Macchia, K. Manoli, C. Di Franco, R. A. Picca, R. Österbacka, G. Palazzo, F. Torricelli, G. Scamarcio, L. Torsi, *ACS Sens.* **2020**, *5*, 1822.
[41] L. Kergoat, B. Piro, M. Berggren, M.-C. Pham, A. Yassar, G. Horowitz, *Org. Electron.* **2012**, *13*, 1.
[42] C. Diacci, M. Berto, M. Di Lauro, E. Bianchini, M. Pinti, D. T. Simon, F. Biscarini, C. A. Bortolotti, *Biointerphases* **2017**, *12*, 05F401.
[43] M. Berto, C. Diacci, R. D'Agata, M. Pinti, E. Bianchini, M. Di Lauro, S. Casalini, A. Cossarizza, M. Berggren, D. Simon, G. Spoto, F. Biscarini, C. A. Bortolotti, M. Di Lauro, S. Casalini, A. Cossarizza, M. Berggren, D. Simon, G. Spoto, F. Biscarini, C. A. Bortolotti, *Adv. Biosyst.* **2018**, *2*, 1700072.
[44] V. Parkula, M. Berto, C. Diacci, B. Patrahau, M. Di Lauro, A. Kovtun, A. Liscio, M. Sensi, P. Samorì, P. Greco, *Anal. Chem.* **2020**, *92*, 9330.
[45] M. Sensi, M. Berto, S. Gentile, M. Pinti, A. Conti, G. Pellacani, C. Salvarani, A. Cossarizza, C. A. Bortolotti, F. Biscarini, *Chem. Commun.* **2021**, *57*, 367.
[46] M. Berto, E. Vecchi, L. Baiamonte, C. Condò, M. Sensi, M. Di Lauro, M. Sola, A. De Stradis, F. Biscarini, A. Minafra, C. A. Bortolotti, *Sensors Actuators, B Chem.* **2019**, *281*, 150.
[47] S. Casalini, A. C. Dumitru, F. Leonardi, C. A. Bortolotti, E. T. Herruzo, A. Campana, R. F. de Oliveira, T. Cramer, R. Garcia, F. Biscarini, *ACS Nano* **2015**, *9*, 5051.
[48] S. Casalini, C. A. Bortolotti, F. Leonardi, F. Biscarini, *Chem. Soc. Rev.* **2017**, *46*, 40.
[49] M. Galliani, C. Diacci, M. Berto, M. Sensi, V. Beni, M. Berggren, M. Borsari, D. T. Simon, F. Biscarini, C. A. Bortolotti, *Adv. Mater. Interfaces* **2020**, *7*, 2001218.
[50] P. A. M. Urbina, M. Berto, P. Greco, M. Sensi, S. Borghi, M. Borsari, C. A. Bortolotti, F. Biscarini, *J. Mater. Chem. C* **2021**, *9*, 10965.
[51] F. N. Ishikawa, M. Curreli, H.-K. Chang, P.-C. Chen, R. Zhang, R. J. Cote, M. E. Thompson, C. Zhou, *ACS Nano* **2009**, *3*, 3969.
[52] J. Meissner, A. Prause, B. Bharti, G. H. Findenegg, *Colloid Polym. Sci.* **2015**, *293*, 3381.
[53] J. G. Lee, K. Lannigan, W. A. Shelton, J. Meissner, B. Bharti, *Langmuir* **2020**, *36*, 14157.
[54] B. Bharti, J. Meissner, G. H. Findenegg, *Langmuir* **2011**, *27*, 9823.
[55] S. Heins, P. C. Wong, S. Muller, K. Goldie, D. W. Cleveland, U. Aebi, *J. Cell Biol.* **1993**, *123*, 1517.
[56] S.-K. Kim, S.-M. Cho, I.-B. Lee, Y. H. Lee, J. H. Kang, J. H. Choi, P.-G. Suh, J.-S. Chang, *J. Neurosci. Methods* **2007**, *161*, 199.
[57] H. Herrmann, R. Foisner, *Cell. Mol. Life Sci. C.* **2003**, *60*, 1607.
[58] K. J. Angelides, K. E. Smith, M. Takeda, *J. Cell Biol.* **1989**, *108*, 1495.
[59] M. K. Lee, Z. Xu, P. C. Wong, D. W. Cleveland, *J. Cell Biol.* **1993**, *122*, 1337.
[60] P. A. Janmey, J.-F. Leterrier, H. Herrmann, *Curr. Opin. Colloid Interface Sci.* **2003**, *8*, 40.
[61] R. Beck, J. Deek, J. B. Jones, C. R. Safinya, *Nat. Mater.* **2010**, *9*, 40.